PROCEEDINGS, Thirty-Second Workshop on Geothermal Reservoir Engineering
Stanford University, Stanford, California, January 22-24, 2007
SGP-TR-183

ANALYSIS OF WELL TESTS IN AFYON ÖMER-GECEK GEOTHERMAL FIELD, TURKEY

Mustafa Onur*, Murat Cinar*, Niyazi Aksoy+, Umran Serpen*, and Abdurrahman Satman*

*Istanbul Technical University, 34469 Maslak, Istanbul, Turkey, +Dokuz Eylul University, 35210 Alsancak, Izmir, Turkey
E-mails: onur@itu.edu.tr, cinarmura@itu.edu.tr, niyazi.aksoy@deu.edu.tr, serpen@itu.edu.tr, mdsatman@itu.edu.tr

ABSTRACT

In this work, analyses of various types of pressure transient tests (such as multi-rate tests, conventional drawdown/buildup tests, and interference tests) conducted in the Afyon Ömer-Gecek geothermal field, Turkey, are presented. The pressure transient tests were conducted at six wells. The pressure data were acquired by downhole quartz gauges, and thus, amenable to the applications of modern well-test analysis techniques such as derivative and deconvolution. Deconvolution analysis based on recently proposed robust algorithms was found useful to extract more information from the variable-rate well tests conducted in the field. In general, the pressure data analyzed indicate that the wells' productivities are quite high, but influenced by non-Darcy flow effects and are producing in a complex fractured/faulted network system. The estimated values of permeability-thickness products (kh) from buildup and interference tests range from 40 to 2000 Darcy-m, whereas porosity-compressibility-thickness products ($\phi c_t h$) estimated from the interference tests range from 2.91×10^{-4} to 1.06×10^{-2} psi/m.

INTRODUCTION

Located in the central Aegean region of Turkey and 15 km northeast of the city of Afyon (Figure 1), the Ömer-Gecek geothermal field is one of the important geothermal fields in Turkey.

The geothermal system can be classified as a low temperature, single-phase liquid-dominated one containing geothermal water (having salinity of 4 000 to 6 000 ppm and dissolved CO_2 content about 0.4% by weight) with temperatures ranging from 50 to 111.6°C. The wells (nearly 30) drilled in the field range in depth from 56.8 to 902 m. The total production rate from the field is about 236 kg/s and the geothermal water produced has been utilized to support a district heating system with a capacity of approximately 4500 residences and some health spa facilities since 1996 (Satman *et al*., 2007).

The Ömer-Gecek geothermal system is a convective hydrothermal type commonly occur in areas of active geological faulting and folding, and areas where the regional heat flow is above normal, as in much of the western Turkey. As for the geology of the system, mica schist and marbles of Paleozoic age forms the basement of the field. At the same time, these rocks form the reservoir system. Neogene deposits composed of conglomerate, sandstone, clayey limestone-sandstone, and volcanic glass-trachandesitic tuff unconformably overlie the Paleozoic basement. A companion paper (Satman *et al.*, 2007) provides further details about the geology, well depths, well temperatures, geochemical analysis of the geothermal water.

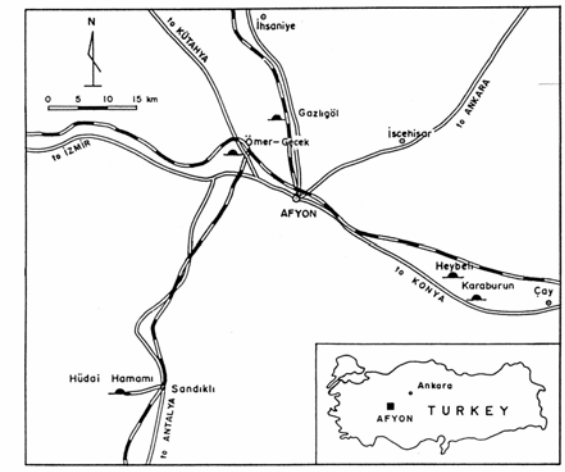

Figure 1. Location map of the Ömer-Gecek geothermal field.

Although the field was explored in 1960s, not much quantitative information on reservoir characteristics (permeability, fault/fracture networks, wells' IPRs etc.), which is essential for understanding and modeling the production performance of the wells and the field, was available. To acquire such information, pressure transient tests were designed and conducted in the field in 2004. Well tests were conducted at six wells; AF-10, AF-11, AF-16, AF-20, AF-21, and R-260. Further information regarding

these wells (location, depth, temperature of the geothermal fluid produced, etc) are given by Satman *et al.* (2007).

The objective of this work is to determine wells' productivities, estimation of permeability-thickness and porosity-compressibility-thickness products, as well as to determine reservoir characteristics (single layer, multi-layer, double porosity, etc.) and reservoir boundaries (faults and their flow characteristics) by the analyses of pressure transient tests conducted in the field.

ANALYSIS OF MULTI-RATE TESTS

Here, we summarize the results obtained from the analyses of multi-rate tests conducted at the wells AF-11, AF-16, AF-20, and AF-21. Multi-rate tests are designed to construct the inflow performance relationship (IPR) of those wells as well as to determine reservoir parameters and characteristics from the pressure signal recorded by using conventional as well as modern well-test analyses techniques based on recently proposed deconvolution algorithms by von Schroeter *et al.* (2004) and Levitan (2005). Only pressure/rate data for the multi-rate test of the well AF-21 and its analysis will be presented here because the multi-rate tests conducted at the other wells give similar behavior to that of AF-21.

The multi-rate test of AF-21 consists of a well-test sequence (4 distinct step rate changes and one shut-in period) acquired over a 16-hour test. Figure 2 presents the pressure and rate data for this well-test sequence (note that a single pressure buildup profile of about 4 hr is acquired at the end of the testing sequence).

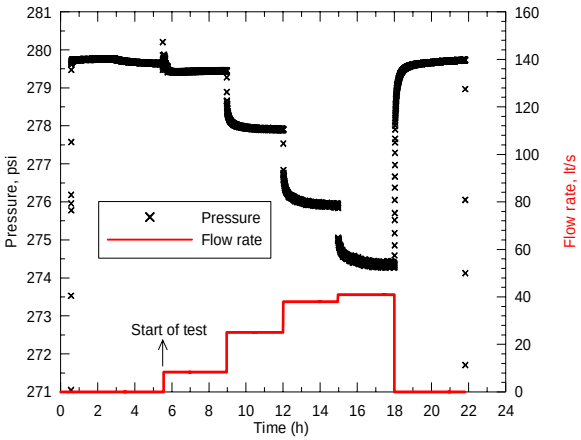

Figure 2. Pressure and rate data for the multi-rate test conducted at the well AF-21.

The pressure measurements shown in Fig. 2 were taken from a down-hole quartz gauge set a depth of 195 m (total depth of the well is 210 m), and rate measurements were taken at the surface using a weir. In this example, the measured initial pressure is about 279.75 psi. Although not shown here, temperatures were also recorded at 195 m during the entire test sequence, and the temperature was nearly constant at 107.8 ^{o}C.

Figure 3 shows the IPR curve obtained from the multi-rate test conducted at the well AF-21. The IPR curve fitted through measured pressure drop data is described best by the steady-state "turbulent" flow model (Eq. 1). The second term bq^2 in the right-hand side of equation is due to non-Darcy flow. The non-Darcy effect observed on the IPR curve of the well AF-21 (as well as on those of other wells tested) is possibly due to a high permeability fracture network system intersecting the well. Because of this, flow rate near the wellbore is so high that the flow regime becomes "turbulent" in the vicinity of the wellbore. Thus Darcy's law loses its validity, and hence the bq^2 term in the right-hand side of Eq. 1 becomes important on well deliverability.

$$\Delta p = aq + bq^2, \qquad (1)$$

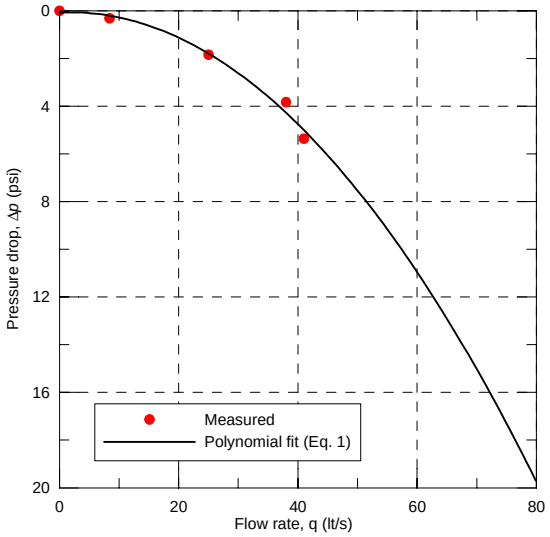

Figure 3. IPR curve for well AF-21, obtained from multi-rate test data shown in Fig. 2.

a and *b* parameters estimated from the multi-rate test for the well AF-21 and for the wells AF-11, AF-20, and AF-21 are given in Table 1. IPR curves constructed for these wells are compared in Figure 4. From Figure 4, it can be seen that IPR curves for all four wells tested indicate a non-Darcy flow model represented Eq. 1 and that the well AF-21 is the most productive amongst four wells.

Table 1. Parameters of IPR curves for Wells AF-11, AF-16, AF-20, and AF-21, determined from multi-rate tests.

Well Name	*a* psi/(lt/s)	*b* psi/(lt/s)^2	p_i (psi) @ depth (m)
AF-11	0.0985	0.00418	147.9 @ 107 m
AF-16	0.0408	0.00276	236.4 @ 174 m
AF-20	0.0249	0.00265	131.8 @ 98 m
AF-21	0.0120	0.00321	279.8 @ 195 m

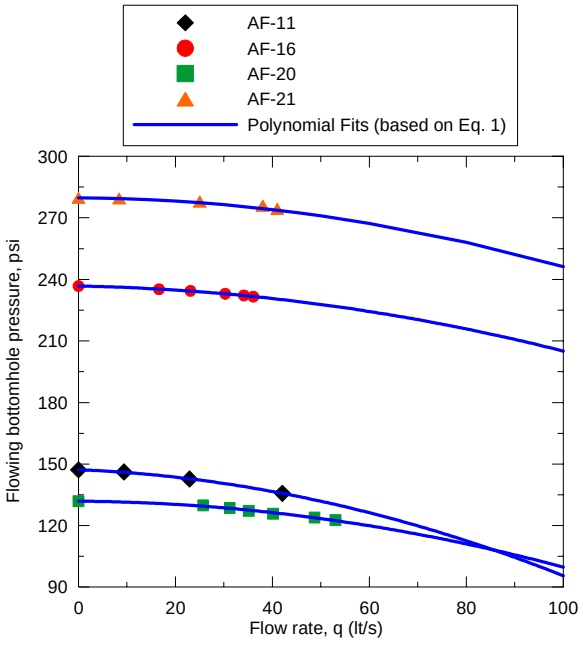

Figure 4. IPR curves for the wells AF-11, 16, 20 and 21, constructed from multi-rate tests.

Although IPR curves and IPR parameters *a* and *b* are useful for understanding the deliverability of wells, and for tubular design purposes, unfortunately, the reservoir parameters such as permeability-thickness product and skin as well as information about reservoir characteristics and boundaries cannot be derived from the "lumped" parameters *a* and *b* of IPR curves. To derive such information, one must analyze the pressure signal, particularly, recorded during the buildup period of multi-rate tests.

Therefore, next, we analyze the pressure signal recorded during multi-rate tests. Here, we will present a detailed analysis only for the multi-rate test of the well AF-21. Figure 5 shows log-log plots of conventional rate normalized multi-rate pressure change vs. elapsed time for each flow period. This graph clearly shows that pressure change data for each flow period are more or less displaced by a constant value. Moreover, as the flow rate increases, the displacement becomes larger. This is possibly due to rate-dependent skin due to non-Darcy flow. Although not shown here, we have also looked at the Bourdet derivatives (Bourdet *et al.*, 1989) for each flow period, these derivative signals indicate changing (and/different) wellbore storage effects (possibly due to non-isothermal/multiphase flow inside the wellbore) at early times of each flow period.

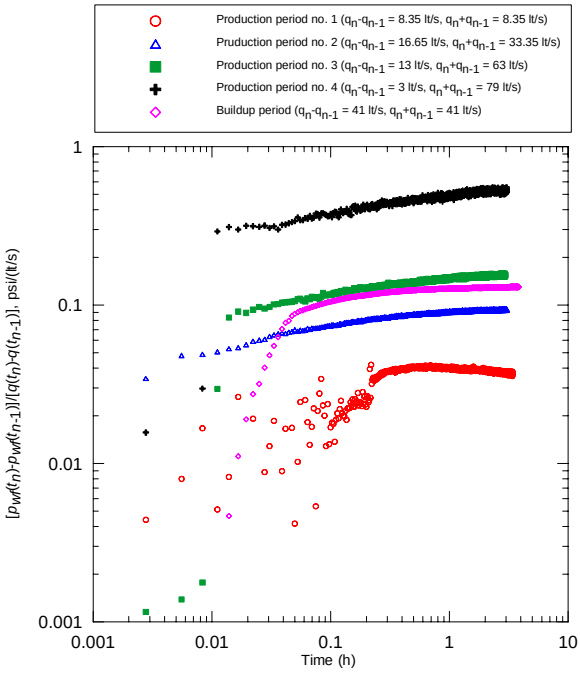

Figure 5. Log-log plot of normalized pressure changes vs. elapsed time for each flow period of the multi-rate test of the well AF-21.

To eliminate the multi-rate effects and convert the multi-rate data into an equivalent unit-rate constant drawdown response, we apply a robust deconvolution algorithm developed by Cinar *et al.* (2006) by accounting for all flow rate history (Fig. 2). As is known (Bourdet, 2002), conventional drawdown or buildup analysis based on superposition-time transform does not completely remove all effects of previous rate variations and often complicates test analysis due to residual superposition effects.

It is worth noting that our deconvolution algorithm used here are based on the ideas presented by von Schroeter *et al.* (2004) and Levitan (2005), and is based on minimization of a weighted least-squares (LS) objective function given by

$$O(z_1, z_2, ..., z_N, q_1^u, q_2^u, ..., q_{N_r}^u, p_0) = \frac{1}{2}\sum_{i=1}^{N_p}\left[\frac{p_0 - p_{m,i} - \Delta p_{model}(t_i)}{\sigma_{p,i}}\right]^2 + \frac{1}{2}\sum_{j=1}^{N_r}\left[\frac{q_{m,j} - q_j^u}{\sigma_{q,j}}\right]^2 + \frac{1}{2}\sum_{k=1}^{N-1}\left[\frac{\kappa_{c,k}}{\sigma_{c,k}}\right]^2 \quad (2)$$

Here, O represents the weighted LS objective function, and the parameters listed in the left-hand side of Eq. 2. Note that the model parameters are the response function z, the rate q, and the initial pressure p_0. Here z is equal to the natural logarithm of the Bourdet derivative of unit-rate drawdown response, that is, $z = \ln[dp_u(t)/d\ln t]$ (where $p_u(t)$ represents drawdown pressure drop if the well were produced at constant unit-rate; see von Schroeter *et al.*, 2004). The rate q plays dual role. It can be treated as one of model parameters. It is also the part of the data that must be fitted to the model.

In Eq. 2, N represents the total number of nodes at which the z-responses to be computed, N_p represents the total number of measured pressure points to be history matched, and N_r is the total number of measured (or allocated) flow rate steps to be treated as unknown in history matching process. It is worth noting that the objective function considered is quite general because it allows one to perform simultaneous estimation of z responses at each node and the initial reservoir pressure p_0, as well as any flow rate steps in the rate sequence. In all applications given in this paper, we use $N = 70$.

In Eq. 2, $\sigma_{p,i}$ represents the standard deviation of error in measured pressure $p_{m,i}$ at time t_i. Typically, in applications, we can assume identically distributed normal errors with zero mean and the same specified standard deviation for each measured pressure point; that is, $\sigma_{p,i} = \sigma_p$; *for* $i = 1, 2, \cdots, N_p$. Levitan (2005) suggests using $\sigma_{p,i} = \sigma_p = 0.01\ psi$ as default value. However, as shown later, if pressure data contain a higher level of noise, then one may need to consider values of σ_p greater than 0.01 psi to obtain a smoother deconvolved unit-rate response. It should be worth noting that if we have noisy data and we require to honor each pressure point by assigning small standard deviation (or equivalently a higher weight) to every pressure point in the objective function, we may end up with noisy deconvolved unit-rate drawdown response function.

Similarly, $\sigma_{q,j}$ represents the standard deviation of error in measured (or allocated) rate step $q_{m,j}$ to be treated as unknown. In our applications given here, we will not treat flow rate data as unknown, and thus the second summation term in the objective function (Eq. 2) is deleted. In Eq. 2, $\sigma_{c,k}$ represents the "standard deviation" of the curvature constraint $\kappa_{c,k}$. As suggested by von Schroeter *et al.* (2004) and Levitan (2005), we set $\sigma_{c,k} = \sigma_c$ for all k, equal to one constant value. We have often found that $\sigma_c = 0.05$ works well. This value has been chosen to provide small degree of regularization and at the same time not to over constrain the problem and create significant bias. In all our applications given here, we use $\sigma_c = 0.05$.

Given the issues of inconsistent data set with the deconvolution model as discussed by Levitan (2005), Levitan *et al.* (2006), and Cinar *et al.* (2006), we will derive deconvolved constant-unit-rate response using only the pressures of the buildup period — and we will assume the rate history is accurate. Our hope is that for this multi-rate test, deconvolution will allow us to better identify the underlying unknown reservoir model and extract more information from the test sequence than that based on the conventional analysis of buildup data based the multi-rate (radial flow) superposition time (Agarwal, 1980). The deconvolved pressure drop and derivative responses obtained from our deconvolution algorithm using three different initial reservoir pressure estimates of 279.75, 279.9 and 280 psi are shown in Fig. 6, and the deconvolution results are compared to the conventional pressure buildup derivatives based the multi-rate (radial flow) superposition time (Agarwal, 1980) plotted versus shut-in time.

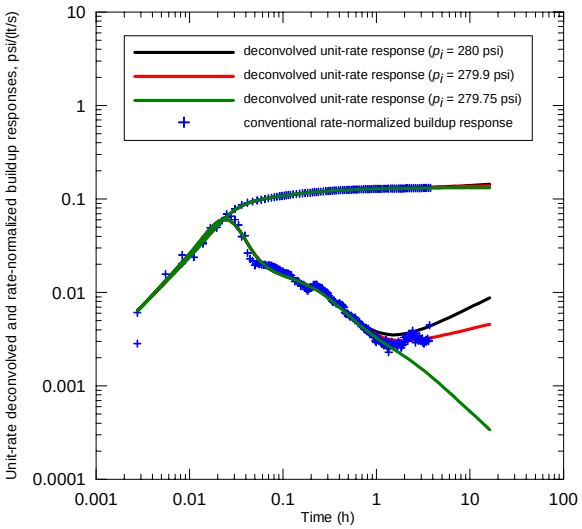

Figure 6. Comparison of deconvolved responses derived from buildup pressures with the conventional pressure buildup pressure change and its Bourdet derivative (normalized by the last rate prior to buildup) for the well AF-21.

The deconvolved responses give an indication of a partially penetrating geothermal well (-1/2 slope line in the interval from 0.07 to 0.2 hr) producing near a highly conductive fault (-1 slope line in the time interval from 0.3 to 1 h). The late time behavior (after 1 h) indicates, however, completely three different flow regimes based on the three different values of initial pressures differing by only 0.25 (max) psi; the one based on 280 psi shows 1/2 slope line indicating a channel or parallel faults, while the one based on 279.9 shows almost 1/4 slope line, indicating a finite conductivity fault (Abbaszadeh, 1995) and the one based on 279.75 psi shows -1 slope line indicating a constant-pressure (or infinite-conductivity) fault.

It is also interesting to note that the conventional rate-normalized buildup pressure change and its derivative data seem to agree better with the deconvolved responses (based on the initial reservoir pressure estimate of 279.9 psi) until 4 h — which is the total duration of the buildup period. Nevertheless, for sure, we cannot determine the correct boundary model based on the deconvolved late time data for this example in high confidence due to sensitivity of deconvolved late-time derivative response (after 4 h) to the initial reservoir pressure. In addition, unfortunately, the geological data available also did not help us to reject one of these boundary models. If we had designed this multi-rate test sequence to include one or more buildup periods, then we would have had the chance to check the validity of the initial pressure by a trial-and-error procedure as suggested by Levitan *et al.* (2006) from deconvolution, and to determine the most appropriate boundary model for the well AF-21.

This example clearly demonstrates how sensitive deconvolution could be to the initial pressure at late time where we actually desire to extract more information about the reservoir model and boundaries than conventional buildup analysis, and emphasize that when designing tests one should consider at least two buildup periods in the test sequence to determine the correct initial reservoir pressure.

Next, we perform parameter estimation for determining permeability-thickness product (kh), skin (s), non-Darcy coefficient (D), and distance to a fault (d_f) by using a "simple" well/reservoir model based on a partially-penetrating (top of the formation is open) well near a constant pressure fault in a homogeneous anisotropic reservoir (i.e., the model indicated by green curves on Fig. 6).

Figure 7 presents a model match of the measured pressure data recorded for the entire multi-rate test sequence. The estimated model parameters are summarized in Table 2. Note that the match is not perfect, particularly, for the second and third flow periods. Nevertheless, in general, the match obtained is acceptable due to possible errors in flow rate data for those flow periods. From Table 2, note that permeability-thickness is quite high, and skin factor is highly negative, indicating a highly permeable fracture or fault zone intersecting the wellbore.

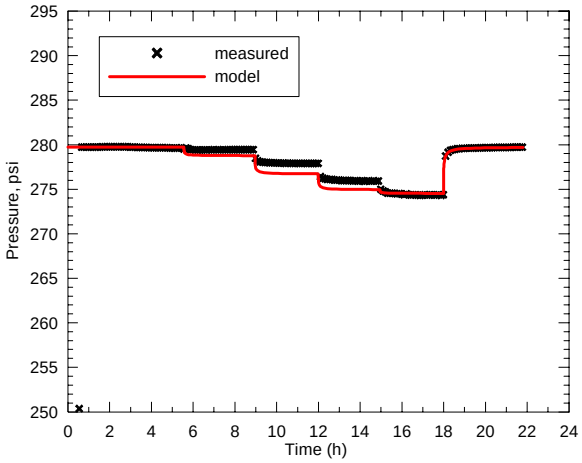

Figure 7. Model match of measured pressure data recorded during entire multi-rate test sequence of the well AF-21.

Table 2. Some input and estimated model parameters for obtaining the model match shown in Figure 7.

Model Parameters	
$k_h h$ (Darcy-m)	308
k_v/k_h (anisotropy ratio)	0.11
p_i, psi	279.72
S (skin, dimensionless)	-5.2
D, $(\text{lt/s})^{-1}$ (non-Darcy coefficient)	$6.5\text{x}10^{-3}$
h_w/h (penetration ratio)length of open interval)	0.385
h_w, m (length of the open interval)	80.8
z_w, m (reservoir thickness)	210
d_f, m (distance to the fault)	177
μ , cp@107.86 ^{o}C	0.27
r_w, m	0.108
$\phi c_t h$ (m/psi)	$2.35\text{x}10^{-4}$

The permeability-thickness (kh), mechanical skin (S), and non-Darcy coefficient (D) values estimated from

multi-rate tests conducted at the wells AF-11, AF-16, AF-20, and AF-21 are summarized in Table 3.

Table 3. kh, S, and D values estimated from multi-rate tests conducted at the wells AF-11, AF-16, AF-20, and AF-21.

Well Name	*kh* (Darcy-m)	*S* dimensionless	*D* $(lt/s)^{-1}$
AF-11	201	-3.3	$8.26x10^{-2}$
AF-16	665	-1.1	$1.92x10^{-1}$
AF-20	1085	-4.3	$4.32x10^{-1}$
AF-21	308	-5.2	$6.5x10^{-3}$

ANALYSIS OF DRAWDOWN/BUILDUP TESTS

Here, we summarize the results obtained from the analyses of conventional drawdown/buildup tests conducted at the wells R-260, AF-11, AF-16, AF-20, and AF-21. A schematic view of the tested well locations together with the other wells in the field, with possible faults given by the geological model, is shown in Figure 8. The red colors in Fig. 8 show the highest elevations (above sea level), whereas dark blue colors show the lowest elevations.

The drawdown/buildup tests are designed to determine *kh*, skin factor, as well as reservoir characteristics and boundaries if possible. Only the drawdown/buildup test of the well R-260 and its analysis will be presented in detail here.

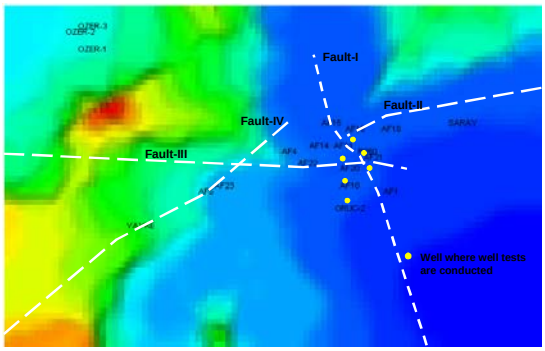

Figure 8. A schematic view showing the wells where well tests are conducted, and possible faults in the field.

Figure 9 presents the pressure/rate recorded during the drawdown/buildup test at the well R-260. The pressure data were measured at a depth of 115 m with a down-hole quartz gauge. The temperature of the fluid recorded at this depth is around 103.6 ^{o}C. The total depth of the well is 166 m. The open interval is from 100 m to 166 m, with 8 and 1/2 inches wellbore diameter. As shown in Fig. 9, the first drawdown period is nearly ten hours at constant production rate of 33.7 lt/s. The duration of the following pressure buildup (PBU) period is 6 hours. After the PBU period, there is another 4-hour flow period with the same flow rate of the first flow period. The total test duration is about 20 hours.

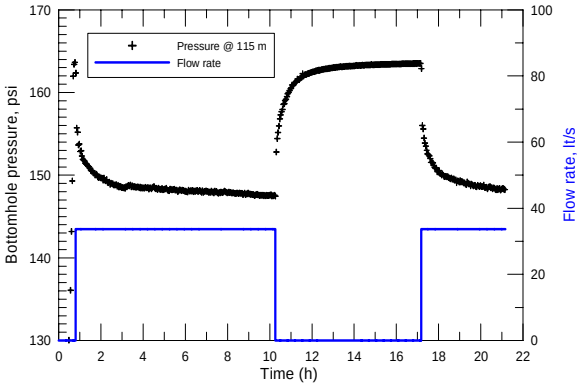

Figure 9. Pressure and rate data for the drawdown/buildup test conducted at the well R-260.

The deconvolved pressure drop (based on PBU data alone) and derivative responses obtained from our deconvolution algorithm are shown in Fig. 10, and the deconvolution results are compared to the conventional pressure buildup derivatives based the conventional (radial flow) Agarwal's superposition time plotted versus shut-in time.

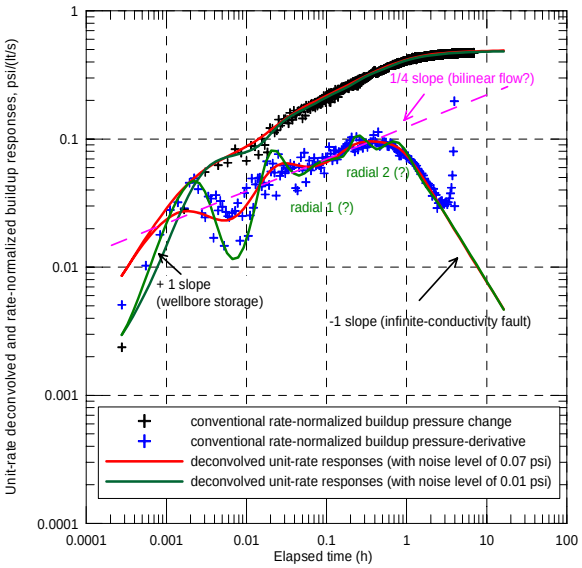

Figure 10. Comparison of deconvolved responses derived from buildup pressures with the conventional pressure buildup pressure change and its Bourdet derivative (normalized by the last rate prior to buildup) for the well R-260.

In deconvolution, we considered two different values of noise level ($\sigma_p = 0.07$ *and* 0.01 *psi* in Eq. 2) for PBU pressures to investigate the effect of noise level on deconvolution (to be discussed below).

The upward trend observed in conventional rate-normalized buildup-derivative data (blue data points in Fig. 10) near the end of buildup period is due to the right-hand side smoothing effect associated by using Bourdet *et al.* (1989) smoothing method with a smoothing parameter L = 0.75. Hence, this upward trend should not be attributed to the reservoir boundary effects. Deconvolved unit-rate responses (red and green curves in Fig. 10) provide a 14-hour longer data set than conventional rate-normalized buildup responses and identify a well-defined -1 slope line for almost one-and-a-half log-cycle near the end of the data, indicating an infinite conductivity (or constant-pressure) fault near the well.

The flow regimes indicated by deconvolved unit-rate derivative data in the time interval from 0.0003 to 1 h are not very conclusive. It seems that deconvolved unit-rate responses for this time period may indicate different flow regimes depending on the noise level used for matching pressure data in deconvolution (see Eq. 2). The deconvolved unit-rate derivative response based on using $\sigma_p = 0.01$ *psi* in Eq. 2 (green curve in Fig. 10) is oscillatory, and indicate changing wellbore storage effects (perhaps, also including possible non-isothermal effects in the wellbore) until 0.1 h, and in the time interval from 0.1 to 1 h, it indicates a radial flow period. The oscillatory behavior of deconvolved data for $\sigma_p = 0.01$ *psi* may indicate that the actual noise level in PBU pressure data could be larger than $\sigma_p = 0.01$ *psi* . To obtain smoother deconvolved data, we tried larger values of noise level for the PBU pressure data to be used in deconvolution, and found that the unit-rate drawdown response generated with a noise level of $\sigma_p = 0.07$ *psi* provides an acceptably smooth curve as shown by red curves in Fig. 10. Although not shown here, unit-rate responses generated with noise levels such that $\sigma_p > 0.07$ *psi* were too smooth to be considered, and root-mean-square (rms) errors for the pressure match obtained for these noise levels were not acceptable.

The deconvolved unit-rate data based on $\sigma_p = 0.07$ *psi* in Figure 10 indicate changing wellbore storage or double porosity behavior in the time period from 0.0003 to 0.01 h, and an intersecting fault (one with no-flow, and other is constant-pressure) for times greater than 0.01 h. Another plausible model is a finite-conductivity fault intersecting the well nearby a constant-pressure fault.

In short, we considered three different plausible models to history match the full pressure history shown in Fig. 9. Model 1 refers to a model with two intersecting faults with a right angle (one is a no-flow, and the other is a constant-pressure). Model 2 refers to a model with a single constant-pressure fault, whereas Model 3 refers to a model with a finite conductivity fracture intersecting the well located near a single-constant pressure fault. The "best" match (based on rms values obtained for the matches, and confidence intervals for parameters) was obtained with Model 1.

Figure 11 presents a model match (based on Model 1) of the measured pressure data recorded for the entire test sequence. The estimated model parameters are summarized in Table 4. As can be seen from Fig. 11, we have almost a perfect match of measured pressure. A highly negative skin factor gives an indication of a highly permeable fracture/fault network intersecting the well.

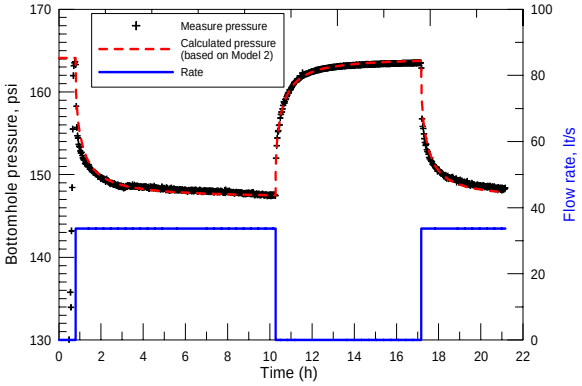

Figure 11. Model match of entire measured pressure data recorded during drawdown and buildup test at the well R-260.

Table 4. Some input and estimated model parameters for obtaining model match shown in Figure 11.

Model Parameters	
kh (Darcy-m)	47.8
p_i, psi	164.09
S (skin, dimensionless)	-4.9
d_{f1}, m (distance to no-flow fault)	63
d_{f2}, m (distance to constant-pressure fault)	126
h, m (formation thickness)	65
μ , *cp*@103.6 ^{o}C	0.281

r_w, m	0.108
$\phi c_t h$ (m/psi)	2.35×10^{-4}

The *kh* and skin factor values estimated from drawdown/buildup tests conducted at the well R-260, AF-11, AF-16, AF-20, and AF-21 are summarized in Table 5. Note that the skin factor values given in Table 5 represents total skin (i.e, $s_t = s + Dq$), including both mechanical skin (s) and non-Darcy skin (Dq). As is known (see, for example, Bourdet, 2002), a constant-rate drawdown/buildup test does not allow one to obtain individual values of mechanical skin and non-Darcy skin (or non-Darcy coefficient, D).

Table 5. Permeability-thickness (kh) and total skin values estimated from analyses of drawdown/buildup tests conducted at wells R-260, AF-11,and AF-16.

Well Name	*kh* (Darcy-m)	*Total skin* dimensionless
R-260	48	-4.9
AF-11	201	1.96
AF-16	665	10.6

ANALYSIS OF INTERFERENCE TESTS

Here, we summarize the results obtained from analyses of two-well interference tests conducted at some of the wells in the field. The well pairs where the interference tests are conducted are AF-21/R-260, AF-21/AF-11, AF-20/AF-10, and AF-20/AF-11. A well name given before the slash indicates an active well, while a well name given after the slash indicates an observation well during the two-well interference test. Here, we only present our analysis for the interference test involved between the wells AF-21 and R-260 in detail. In this test, AF-21 is the active well, while the well R-260 is the observation well. The distance between the two wells is 78.5 m.

Figure 12 presents flow-rate history at the active well (AF-21) and pressure recorded at the observation well (R-260). The bottomhole pressure at the well R-260 was recorded at a depth of 116 m by a downhole quartz gauge.

Although it is not evident from Fig. 12, the production at AF-21 is felt at R-260 in 100 seconds, indicating a highly permeable fracture/fault network existing between the wells. The total test duration after production started at well AF-21 is about 170 h (or about 7 days). The static pressure measured at the well R-260 at the depth of 116 m is 158.5 psi. After first 140 hours of production at AF-21, the well R-260 was shut-in about 6 hours due to some operational problems occurred at the well AF-21. This shut-in period provided a 6-hour buildup test data in the time interval from 182 to 188 h (in cumulative time) as shown Fig. 12.

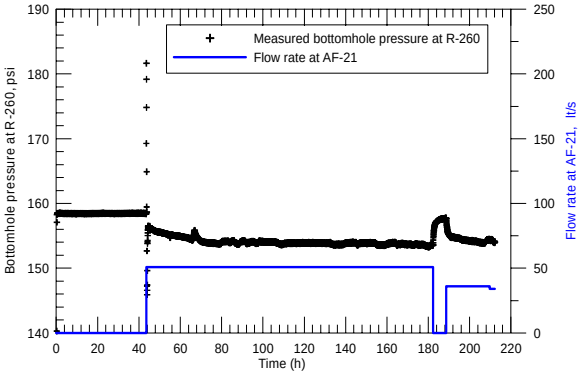

Figure 12. Pressure and flow rate history for the AF-21/R-260 two-well interference test.

In Figure 13, we present the deconvolved responses (pressure drop and derivative functions) derived from the buildup pressures, and we compare these results with the conventional normalized buildup pressure-change and its derivative with respect to Agarwal's equivalent time plotted versus elapsed time. In deconvolution, we considered two different values of initial reservoir pressure; one is 158.5 psi (as the measured value), and the other is 157.93 psi. We assume that the flow rate history prior to buildup is accurate and can be treated as known in deconvolution procedure of Eq. 2. In all deconvolved responses, we set the noise level in PBU data as σ_p = 0.01 psi.

Although deconvolution provides about a one-and-a-half cycle longer data than conventional rate-normalized buildup data, the late portions of deconvolved responses indicate two different model behaviors due to its sensitivity to the value of initial pressure. As we do not have another buildup period, we do not know for sure which value of the initial pressure is the appropriate value. If we accept that the measured value of p_i = 158.5 psi is the appropriate one, then the late-time portion of deconvolved unit-rate derivative response (green curves in Fig. 13) gives an indication of a finite-conductivity fault near the well, whereas if we accept that p_i = 157.93 psi is the appropriate one, then the late-time portion of deconvolved unit-rate derivative response (red curve in Fig. 13) indicates a constant-pressure (or infinite-conductivity) fault.

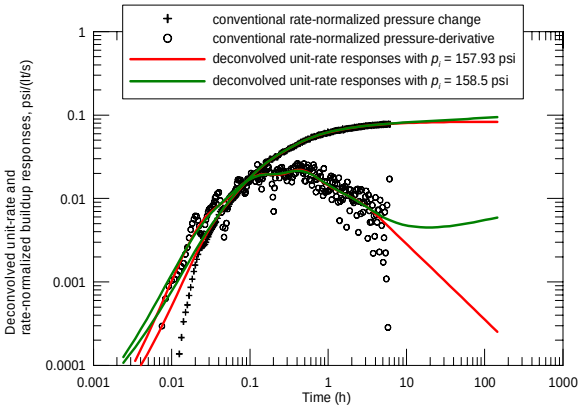

Figure 13. Comparison of deconvolved responses derived from buildup pressures with conventional pressure buildup pressure change and its Bourdet derivative (normalized by the last rate prior to buildup).

Next, we perform parameter estimation for determining permeability-thickness product (kh) and porosity-compressibility-thickness product ($\phi c_t h$), and the distance (r_i) between the observation well R-260 and an imaginary well by using a "simple" well/reservoir model considering a fully-penetrating well near a constant-pressure fault in a homogeneous isotropic reservoir (i.e., the model indicated by red curves on Fig. 13). Figure 14 presents a model match of the measured pressure data recorded for the entire interference test sequence, and the match can be considered as acceptable.

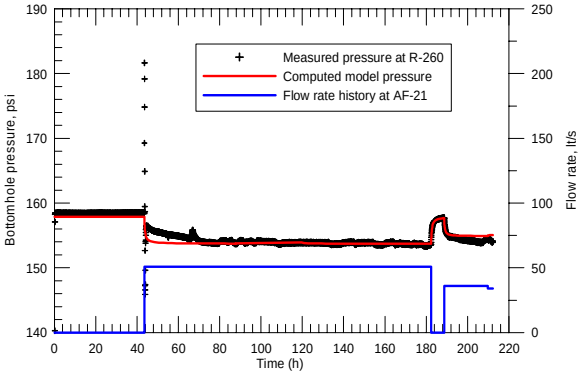

Figure 14. Model match of entire measured pressure data recorded at the well R-260 during AF-21/R-260 interference test.

The estimated model parameters are summarized in Table 6. It is important to note that r_i given in Table 6 represents the distance between the well R-260 and an imaginary well, perpendicular to the fault. As is known from the work of Vela (1977), one cannot determine uniquely the distance to the fault and its orientation from a single-interference test. Note also that kh value estimated from this interference test is different from kh values estimated from the tests where AF-21 and R-260 were pulsing wells alone (see Tables 2 and 4). These results as well as the results given in Table 7 indicate that the geothermal reservoir under consideration is highly heterogeneous and permeable. In addition, interference tests give an indication that permeability is more developed in the NS direction than in the EW direction.

Table 6. Some input and estimated model parameters for obtaining model match shown in Figure 14.

Model Parameters	
kh (Darcy-m)	135
p_i, psi	157.93
r_i, m (distance between the well R-260 and an imaginary well)	382
h, m (formation thickness)	65
μ , cp@103.6 ^{o}C	0.281
r_w, m	0.108
$\phi c_t h$ (m/psi)	2.91×10^{-4}

The permeability-thickness (kh) and the porosity-compressibility-thickness ($\phi c_t h$) products estimated from all interference tests conducted in the field are summarized in Table 7.

Table 7. kh and $\phi c_t h$ values estimated from two—well interference test conducted in the field.

Well Pairs Active/observation	kh (Darcy-m)	$\phi c_t h$ (m/psi)
AF-21/R-260	135	2.91×10^{-4}
AF-21/AF-11	610	2.98×10^{-3}
AF-20/AF-10	1900	1.06×10^{-2}
AF-20/AF-11	415	2.00×10^{-3}

CONCLUSIONS AND RECOMMENDATIONS

In this work, we presented analyses of various types of pressure transient tests (such as multi-rate tests, conventional drawdown and buildup tests, and interference tests) conducted in the Afyon Ömer-Gecek geothermal field, Turkey. In general, the pressure tests analyzed indicate that the wells' productivities are quite high, but influenced by non-

Darcy flow effects and are producing in a complex fractured/faulted network system. The estimated values of permeability-thickness products (*kh*) from multi-rate, drawdown/buildup and interference tests range from 40 to 2000 Darcy-m. The well test data also identify highly conductive (recharging) faults, where we believe these faults are dominating the performance of the geothermal field. Regarding determining these faults orientations in the field, additional pressure transient tests and more detailed geological and geophysical work are recommended.

Deconvolution analysis based on recently proposed robust algorithms by von Schroeter *et al.* (2004) and Levitan (2005) was found useful to extract more information from the well tests conducted in the field. However, it should be stated that deconvolved responses can be quite sensitive to noise level in pressure data and the initial reservoir pressure. Hence, characterizing and estimating the appropriate noise level in pressure *a priori* and designing tests that include at least two buildup periods to identify the appropriate initial reservoir pressure are recommended to accurately and properly interpret the results derived from such deconvolution algorithms.

ACKNOWLEDGEMENTS

We thank the management of AFJET A.Ş. for giving us the permission to use the pressure data presented in this study. The pressure tests were conducted by Iller Bank of Turkey.

REFERENCES

Abbaszadeh, M. and Cinco-Ley, H. (1995), "Pressure Transient Behavior in a Reservoir With a Finite-Conductivity Fault," *SPE Formation Evaluation* (March) 26.

Agarwal, R.G. (1980), "A New Method to Account for Production Time Effects When Drawdown Type Curves Are Used to Analyze Buildup and Other Test Data," paper SPE 9289 presented at the 1980 SPE Annual Technical Conference and Exhibition, Dallas, TX, 21-24 September.

Bourdet, D. (2002), *Well Test Analysis: The Use of Advanced Interpretation Models*, Elsevier, Amsterdam, the Netherlands, 426 pp.

Bourdet, D., Ayoub, J.A., and Pirard, Y.M. (1989), "Use of Pressure Derivative in Well-Test Interpretation," *SPE Formation Evaluation* (June) 69.

Cinar, M., Ilk, D., Onur, M., Valko, P. P., Blasingame, T. A. (2006), "A Comparative Study of Recent Robust Deconvolution Algorithms for Well-Test and Production-Data Analysis," Proceedings, *the 2006 SPE Annual Technical Conference and Exhibition*, San Antonio, Texas, September. 24-27.

Levitan, M.M. (2005), "Practical Application of Pressure/Rate Deconvolution to Analysis of Real Well Tests," *SPE Reservoir Evaluation and Engineering* (April) 113.

Levitan, M.M., Crawford, G.E., and Hardwick, A. (2006), "Practical Considerations for Pressure-Rate Deconvolution of Well-Test Data," *SPE Journal* (March) 35.

Satman, A., Onur, M., Serpen, U, Aksoy, N. (2007), "A Study on the Production and Reservoir Performance of Omer-Gecek/Afyon Geothermal Field," Proceedings, *Thirty-Second Workshop on Geothermal Reservoir Engineering*, Stanford University, Stanford, California, Jan. 22-24.

Vela, S. (1977), "Effect of a Linear Boundary on Interference and Pulse Tests-The Elliptical Influence Area," *Journal of Petroleum Technology* (August), 947.

von Schroeter, T., Hollaender, F., and Gringarten, A.C. (2004), "Deconvolution of Well Test Data as a Nonlinear Total Least Squares Problem," *SPE Journal* (December) 375.